ADVANCED MATERIALS
www.advmat.de

A Single-Molecule Memristor based on an Electric-Field-Driven Dynamical Structure Reconfiguration

Yilin Guo, Chen Yang, Shuyao Zhou, Zhirong Liu, and Xuefeng Guo**

A robust single-molecule memristor is prepared by covalently integrating one phenol molecule with multiple binding sites into nanogapped graphene electrodes. Multilevel resistance switching is realized by the electric-field-manipulated reconfiguration of the acyl moiety on the phenol center, that is, the Fries rearrangement. In situ measurements of the reaction trajectories with an initial single substrate and an intermediate break through the limitation of macroscopic experiments, therefore unveiling both intramolecular and intermolecular mechanistic pathways (a long-term controversy) as well as comprehensive dynamic information. Based on this advance, high-performance single-molecule memristors in both the solution and solid states are achieved successively, providing a new understanding of memristive systems and neural network computing.

1. Introduction

The development of memristive devices is regarded as a promising technology for continuing Moore's law.[1] The characteristics of self-triggered (source–drain voltage) inherent resistance variations in the simplest two-terminal structure enable memristors to be integrated with a higher density and lower fabrication cost, which meets the demands of device miniaturization and supercomputing, as well as non-traditional brain-inspired computing.[2,3] In recent years, scientists have made progress in device miniaturization, especially memristor arrays at the nanoscale.[4–9] However, the memristors are still in an early phase of development.[10,11] To further optimize the technical indicators, including feature size, long-lasting retained memory states, write–erase endurance, working frequency, and on/off ratio,[12] we report a reliable memory effect of one molecule derived from dynamical structure reconfiguration rather than typical electrochemical doping or charge trapping.[13] The relatively high energy barriers among the different molecular structures provide a stable memory state. In addition, owing to the close relationship between the molecular structure and its conductance, the desired resistance can be precisely designed by molecular engineering in organic synthesis to realize tunable on/off ratio multilevel behaviors. Therefore, memristors built using single molecules are particularly attractive, showing a small physical size, high performance, and integration capability.

Numerous types of single-molecule devices have been demonstrated in previous studies, including switch,[14] field-effect transistor,[15,16] rectifier,[17] single-photon source,[18] and electrets.[19] Meanwhile, dynamic monitoring of the focused single molecule provides unique insights into the reaction chemistry from the bottom space, including the hidden intermediate,[20] reaction pathway,[21] and dynamic disorder.[22] Although many reaction mechanisms are well defined through adequate macroscopic evidence, the clarification of numerous uncertain reaction mechanisms requires a full understanding at the molecular level, such as Fries rearrangement,[23] which is a valuable organic synthesis method.[24] In this study, the dynamic structure reconfiguration in this reaction was directly observed and precisely manipulated at the single-molecule level to clarify the inherent mechanism with a long-standing controversy, develop electric-field-driven catalysis, and be applied for memory applications (**Scheme 1** and **Figure 1**).

Specifically, divergent perspectives about the mechanistic pathway, including completely intramolecular,[25–27] completely intermolecular,[28–30] and partially intra- and intermolecular[31–33] were proposed after inconsistent macroscopic crossover experiments[25] (Figure S2, Supporting Information). To this end, an individual molecule needs to be captured and focused on during its reaction (a detailed discussion is provided in Section S3, Supporting Information). The characterization of intra- and intermolecular interactions during the reaction with insights from only one molecule can undoubtedly suppress cognition at the ensemble level. In this study, a single molecule was covalently integrated into nanogapped graphene electrodes to form a stable graphene-molecule-graphene single-molecule junction (GMG-SMJ). This junction can track the pathway of the Fries rearrangement in real time and its specific intramolecular/intermolecular interaction mode, which elucidates the controversial reaction mechanism and provides a powerful tool for

Y. Guo, C. Yang, S. Zhou, Z. Liu, X. Guo
Beijing National Laboratory for Molecular Sciences
National Biomedical Imaging Center
College of Chemistry and Molecular Engineering
Peking University
292 Chengfu Road, Haidian District, Beijing 100871, P. R. China
E-mail: LiuZhiRong@pku.edu.cn; guoxf@pku.edu.cn
X. Guo
Center of Single-Molecule Sciences
Institute of Modern Optics
Frontiers Science Center for New Organic Matter
College of Electronic Information and Optical Engineering
Nankai University
38 Tongyan Road, Jinnan District, Tianjin 300350, P. R. China
The ORCID identification number(s) for the author(s) of this article can be found under https://doi.org/10.1002/adma.202204827.

DOI: 10.1002/adma.202204827

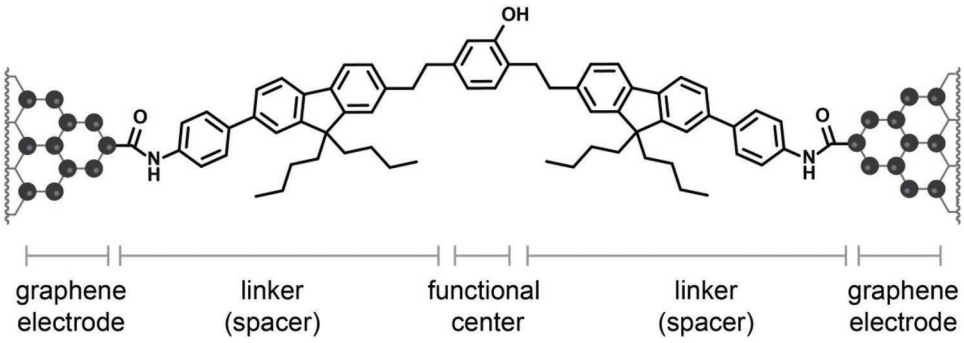

Scheme 1. Schematic illustration of a phenol-based single-molecule junction, showing the structural details of each part.

future molecular interaction studies. In addition, the external electric field (EEF) provided by the applied bias voltage for GMG-SMJs can effectively regulate the reaction energy barrier, realizing a new-generation mode of manipulation, effective switching between different states, and stabilization of only one desired state, which meets the needs of current memristors.

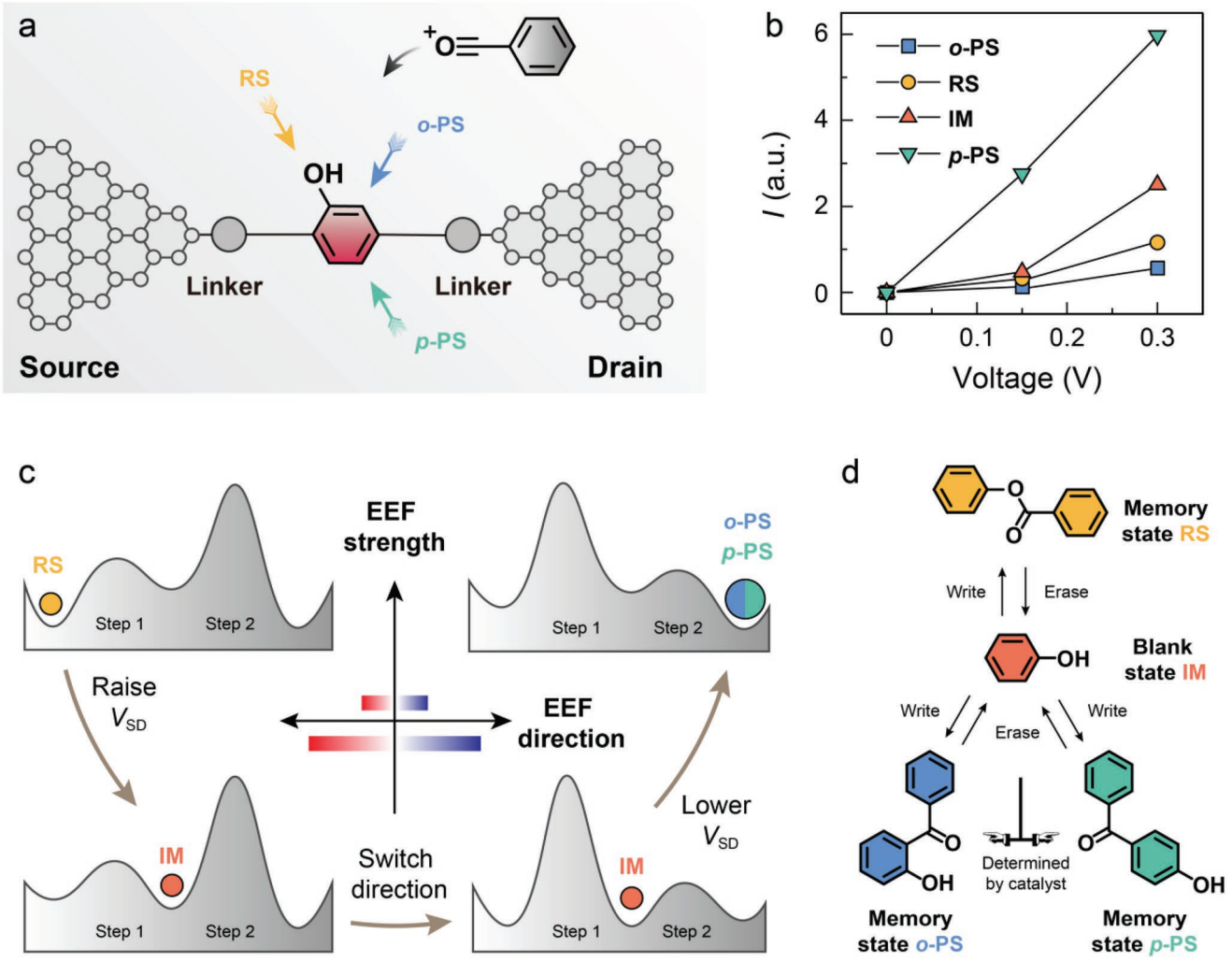

Figure 1. Schematic of the single-molecule memristor and the resistance switching via single-molecule Fries rearrangement. a) Schematic demonstration of the working principle for a phenol-based single-molecule memristor. Two linkers are connected to the phenol to decouple the functional center from the electrodes. Two sites on the phenol center for reconfiguration of the acyl moiety contribute to varied resistance. b) Simulated *I*–*V* curves of four species involved in the Fries rearrangement. c) Regulation of the energy profile and manipulation of the species by EEFs. d) Schematic of the write–erase progress on single-molecule memristors. RS, reactant state; IM, intermediate state; *o*-PS, *ortho*-product state; *p*-PS, *para*-product state; V_{SD}, source–drain voltage; EEF, external electric field.

2. Fabrication of Single-Molecule Memristors

In view of molecular engineering, a molecular bridge with a phenol functional center (the precursor of the substrate as well as the intermediate of the reaction) and the amino terminals was integrated into carboxyl-terminated graphene point electrodes via amide bonds to form a GMG-SMJ (Scheme 1 and Figure 1a). The molecular synthesis and process of device fabrication are provided in the Supporting Information (Schemes S1 and S2, Figure S1, Supporting Information). The current–voltage (*I*–*V*) response indicates the successful formation of single-molecule devices (Figure S3, Supporting Information). Under optimized conditions, approximately 12 of the 126 devices exhibited an *I*–*V* response (≈10% connection probability) (Figure S4, Supporting Information). The probability of connecting only one molecule between a pair of electrodes was approximately 95% according to the binomial distribution analysis (refer to Section S5, Supporting Information), which has also been proven by previous reports using a home-made photoelectric coupled instrument system.[20,21]

After esterification of the phenol center (Figure S5, Supporting Information), the Fries rearrangement, that is, the dynamical reconfiguration of the acyl moiety on phenol, can be monitored. The source of the acyl moiety that attacks the benzene ring, including the self-one on the functional center or the other in the solution, could be identified through electrical characterization (Figure S2a, Supporting Information), which sheds light on the intra-/intermolecular pathways (Figure S2b, Supporting Information). As the dominant electron transmission channel, the different binding sites can be determined by the corresponding conductance over a wide bias voltage range (Figure 1b and Figure S2c, Supporting Information). The reconfiguration of the acyl moiety leads to variations in device resistance.

3. Regulation of Fries Rearrangement via EEFs for the Memristive Operation in Solution

In the presence of the 1×10^{-8} mol L^{-1} catalyst, phenyl benzoate (1×10^{-8} mol L^{-1}) in dichloroethane solution was added to the homemade reaction cell containing the molecular bridge (where $TiCl_4$ leads to *ortho*-product, polyphosphoric acid to *para*-product, or CF_3SO_3H to the mixed product). In the presence of CF_3SO_3H, different switching models in the *I*–*t* curves were recorded under positive or negative bias voltages at 358 K (Figure S6, Supporting Information, and **Figure 2**a; the recorded signals in the presence of $TiCl_4$ and polyphosphoric acid, respectively, are provided in Section S8, Figures S7–S10, Supporting Information). Two conductance states were recorded under a positive bias, whereas three conductance states were observed under a negative bias. Owing to the symmetrical *I*–*V* curve of bare phenol in the bias range from −500 to +500 mV (Figure S3, Supporting Information), the different models of the *I*–*t* curves exhibited different reaction behaviors, implying a certain regulatory effect on the reaction by EEFs.[34,35]

The influence of EEFs on the potential energy surface of the Fries rearrangement was simulated to explain this phenomenon (Figure 1c and Figures S11–S17, Supporting Information; the theoretical methods are provided in Section S9, Supporting Information). The intensity and direction of the electric field (parallel to the direction of the molecular bridge) had a regular and obvious influence on the potential energy surface of the reaction (the representative structures and corresponding direction of the EEFs are shown in Figures S18 and S19, Supporting Information). The entire reaction pathway can be described by a two-step process (Figure 1c): phenyl benzoate state (RS) to phenol intermediate (IM) (Step 1) followed by IM to the product state (PS) (Step 2). A positive EEF lowers the energy barrier of Step 1 but inhibits Step 2. The occupancy of RS and IM in Step 1 was also regulated by the EEF strength. In contrast, a similar regulation of favored Step 2 in the negative EEF, which supports the difference in *I*–*t* curves with the bias voltage in the opposite direction, was obtained. Therefore, by combining the potential energy surface and species transition sequence, all conductance states can be reasonably assigned (Figure S6, Supporting Information, and Figure 2a). The same conductance state that appeared under both positive and negative biases was assigned to IM phenol (red). The lower conductance state under positive bias was assigned to RS phenyl benzoate (yellow), while the highest and lowest conductance states under negative biases were assigned to the corresponding products (*o*-PS (blue) and *p*-PS (green)), according to the electron transmission spectra in Figure 1b (detailed discussion is provided in Sections S11 and S12, Figures S20–S24, Supporting Information). These assignments were also supported by the inelastic electron tunneling spectra (IETS, Figure S32, Supporting Information; the corresponding molecular models for the IR and Raman spectrum simulations are provided in Figure S33, Supporting Information). Owing to the relatively high energy barriers of both Steps 1 and 2 without EEF, the RS and PS (with different resistances) can be regarded as a nonvolatile storage state, and the write–erase operation between them can be realized by applying bias voltage inputs (Figure 1c,d).

To further study EEF regulation and demonstrate the write–erase operation, bias-voltage-dependent measurements were conducted, as shown in Figure 2a. In the positive range (≈0.05–1 V (left panel), stochastic switching between RS and IM was monitored and the RS was stable without bias voltage or at lower electric inputs (<0.1 V), while the IM can be enriched at high bias voltages. In contrast, stochastic switching between PS and IM was monitored in the negative bias range (≈−0.05—1 V, Figure 2a, right panel), involving stable PS at lower (no) electric inputs and polarized IM at higher biases. Therefore, RS and PS are stable under natural conditions, while high EEFs induce cleavage of the C—O bond and stabilize IM. To date, we have split a complex Fries rearrangement into two simple elementary reactions through an electric field to study separately (including the inherent thermodynamic and kinetic characteristics, refer to the Supporting Information, Sections S13 and S14, Figures S25–S29, Supporting Information), which are difficult to achieve in macroscopic experiments (only continuous reaction processes can be monitored). Keeping the reaction in a certain stage could be realized via the regulation of the electric field, which provides a useful tool to simplify the reaction and reflects the advantages of single-molecule electrical detection.

A repeatable switch between stable RS and PS can be realized with a well-designed electric input sequence, which shows

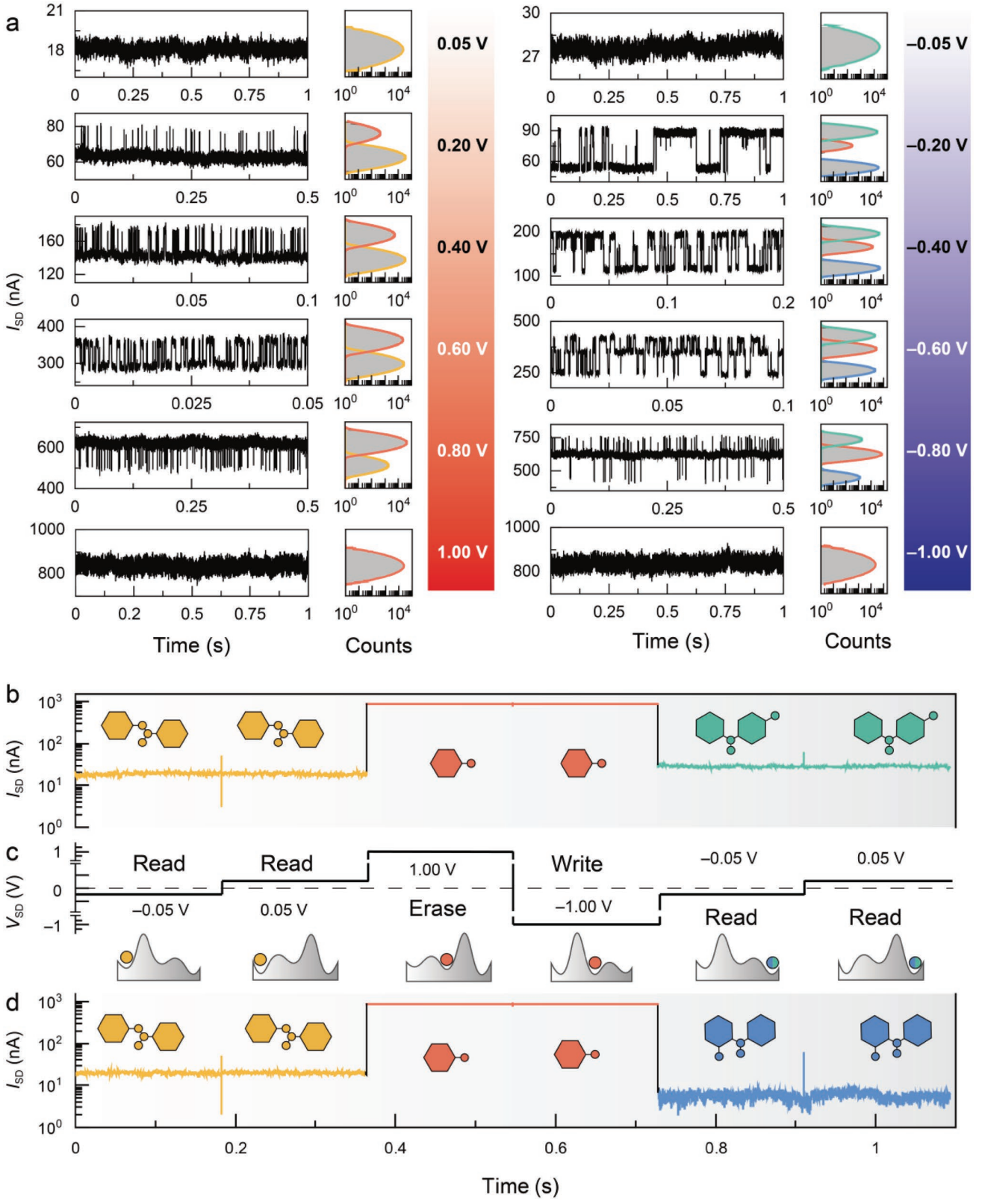

Figure 2. Regulation of Fries rearrangement via EEFs for the memristive operation in solution. a) *I–t* curves and corresponding histograms in the bias-voltage-dependent measurement. b) Recorded current signals during the read–erase–write–read operation to the single-molecule memristor with the catalysis by polyphosphoric acid. c) Applied operation voltages and schematic of the corresponding state on the energy profile. d) Recorded current signals during the read–erase–write–read operation to the single-molecule memristor with the catalysis by $TiCl_4$.

the characteristics of the write–erase operation (Figure 2b–d and Figure S30, Supporting Information. The corresponding *G*–*t* curves in Figure 2b–d are shown in Figure S31, Supporting Information). The initial stable state, RS (*p*-PS), can be read with a lower electric input (≈–0.05–+0.05 V, Figure 2b,c). These states can be erased to the IM by a +1 V (–1 V) high-level electric input. Then, it can be written to another stable *p*-PS (RS) by an opposite –1 V (+1 V) electric input and polyphosphoric acid catalysis because of the preference for negative (positive) EEFs for Step 2 (Step 1) (Figure 2b,c). Note that a lower opposite electric input like –0.05 V (+0.05 V) can also realize the writing operation. The written new state can also be read by a lower electric input (–0.05 to +0.05 V) (Figure 2b,c). Multilevel switching can be achieved using two binding sites (*ortho*- or *para*-) in the phenol center for the reconfiguration of the acyl moiety (corresponding to different resistances). The write–erase switching between the RS and *o*-PS is shown in Figure 2c,d. The written state can be permanently reserved due to the high energy barrier for both Steps 1 (≈17.8 kcal mol^{-1}) and 2 (≈19.3 kcal mol^{-1}) without electric inputs (Figure S11, Supporting Information). Long-term write–erase endurance can also be obtained owing to the stable covalent interface[36] between the single molecules and electrodes (Figure S30, Supporting Information). The microsecond-level (less than the time resolution of the instrument) writing speed results from the corresponding decreased energy barriers (reconfiguration of the acyl moiety in the Fries rearrangement), which shows application prospects in high-frequency devices. Meanwhile, the high writing speed excludes the diffusion-controlled reaction process to some extent, which implies intramolecular progress of the Fries rearrangement.

4. Clarification of the Fries Rearrangement Mechanism

To further clarify the uncertain (intra- or intermolecular) mechanism of the Fries rearrangement, in situ measurements of a single substrate and intermediate were designed. Additionally, the interaction between the acyl moiety and phenol center can be characterized by concentration-dependent measurements, which break through the bottleneck of macroscopic experiments (the same substance cannot be described using the concentration variable). Considering the single-substrate-molecule measurement (without additional substrates), only the esterified functional center (RS) of the molecular bridge was focused on in the CF_3SO_3H solution. After the application of a bias, several events of conductance binary switching were monitored, followed by a stable state (**Figure 3**a, +0.3 V), implying several events of structural reconfiguration between RS and IM. The control experiment with an unesterified single-phenol-molecule device excluded other interferences (Figure S34, Supporting Information). The latter stable conductance state was attributed to phenol (IM) owing to the same conductance as the initial phenol (≈33 nA, which was supported by IETS, Figure S32, Supporting Information). A similar electrical signal was obtained with the re-acylated device, which supported this assignment. Similar phenomena (ternary switching among IM, *o*-PS, and *p*-PS followed by a stable IM) were also observed at –0.3 V. Common to both the positive and negative biases in several events of acyl moiety reconfiguration on phenol center followed by leaving into the solution. The reversibility was attributed not only to the similar thermodynamic preference in the reaction coordinate (Figure 1c) but also to the temporary stay of the acyl owing to the π-cation interaction.[37] There is almost no chance for the escaped acyl moiety to return to the center, which leads to the long-term occupancy of the IM. Therefore, based on monitoring the rearrangement trajectories of a focused substrate, the intramolecular pathway can be determined, and the complete intermolecular route can be excluded. Furthermore, the eigenvalues of the events describing the acyl moiety reconfiguration can be obtained from multiple sets of trajectories, showing the inherent static energy profile and dynamic behaviors of the Fries rearrangement (refer to Section S19, Figures S35 and S36, Supporting Information). These were hardly detected macroscopically and added further insights into the dynamic disorder in the single-molecule reaction.

The existence of an intermolecular pathway was demonstrated by single-intermediate-molecule measurements (without esterification of the phenol functional center), monitoring its behavior in the presence of other substrates (1×10^{-8} mol L^{-1}) in solution. Similar electrical signals were obtained under positive (binary switching, +0.3 V) and negative (ternary switching, –0.3 V) biases (Figure S37, Supporting Information), implying Steps 1 and 2, respectively. Additionally, the quantitative kinetic and thermodynamic analyses (Figure S37, Supporting Information) were in good agreement with the routine measurements of the esterified single-phenol device under the same conditions (refer to the quantitative rate estimation in Section S23, Figures S43 and S44, Supporting Information). The monitored reaction trajectories from the initial bare phenol to the corresponding rearrangement product revealed an intermolecular pathway for the selected reaction system, and the complete intramolecular route was excluded. The focus on one intermediate molecule at the microscopic level also resulted in direct observation of the interaction in the rearrangement and complementary comprehension, which may inspire a new generation of methodologies for studying organic mechanisms.

In addition, concentration-dependent measurements provided evidence for both intra- and inter molecular pathways. Varied *I*–*t* curves versus different substrate concentrations under negative and positive biases (the long-term data, corresponding statistical results, and analysis are provided in Figures S38–S44, Supporting Information) indicate an intermolecular reaction path (Figure 3c shows the interaction between the acyl moiety and the phenol center in the presence of other substrate molecules). The proposed conversion relationship, including the intra- and intermolecular pathways, is shown in Figure 3d. Based on the steady-state approximation (Equations (1) and (2)), the ratios of [RS]/[IM] and [PS]/[IM] showed a theoretical linear relationship with the substrate concentration [A]. This can be verified experimentally in the low-concentration range (Figure 3e), while saturated substrate molecules around the reaction center lead to a non-obvious impact on the reaction at a high concentration range (Figure S42, Supporting Information). The corresponding derived intercepts according to the linear fitting represent the reaction thermodynamic characteristics extrapolated to the 0 mol L^{-1} substrate, that is, the single-substrate reaction, which agrees with the

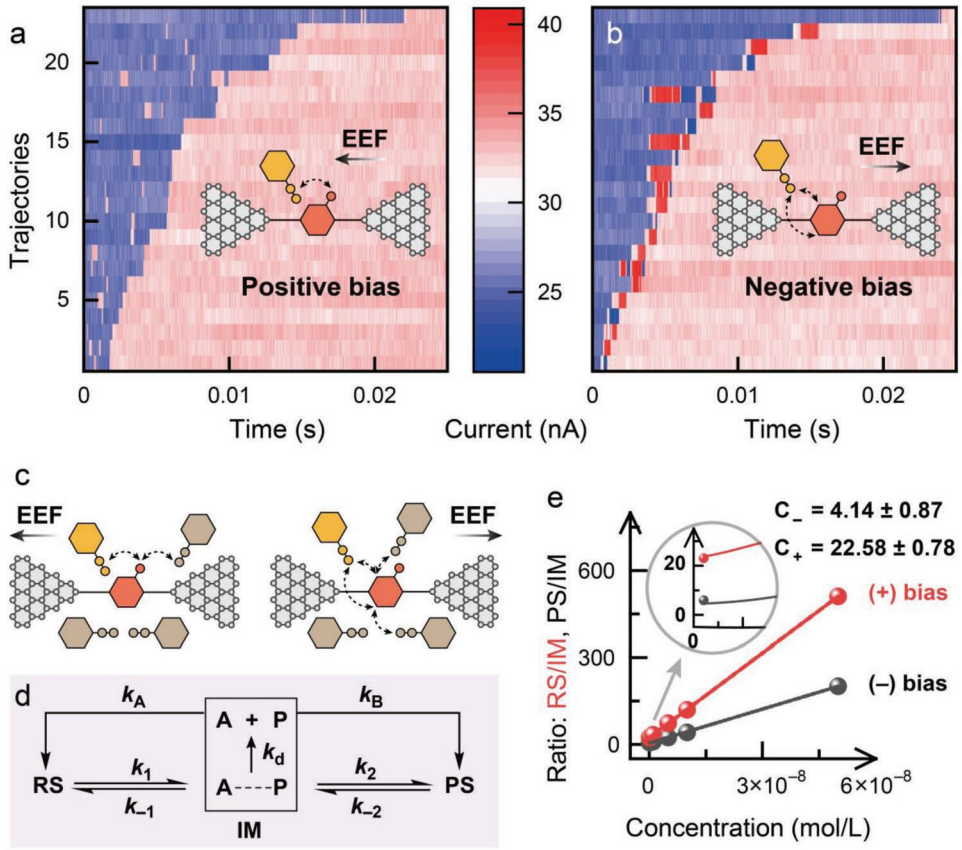

Figure 3. Clarification of the Fries rearrangement mechanism. a) Mapping of *I–t* curves in 23 sets of single-substrate-molecule measurements and dynamic analysis at +0.3 V. Inset: Schematic of the switching between RS and IM. b) Mapping of *I–t* curves in 23 sets of single-substrate-molecule measurements and dynamic analysis at –0.3 V. Inset: Schematic of the switching between PS and IM. c) Schematic of the interaction between the acyl moiety and the phenol center with the existence of other substrate molecules. d) Schematic of the rate conversion in the Fries rearrangement. e) Plots of ratio versus concentration at positive and negative biases (Figures S38–S41, Supporting Information), which are fitted with linear lines, and the corresponding intercepts. The part closed to the *y*-axis was enlarged in the gray circle.

corresponding parameters derived from Figure 3a,b, implying the existence of an intramolecular pathway (a detailed discussion is provided in Section S22, Supporting Information). Therefore, the partial intra- and intermolecular mechanistic pathway of the Fries rearrangement was supported by the single-substrate/intermediate-molecule measurements as well as the concentration-dependent measurements on the single-molecule device.

$$\frac{[RS]}{[IM]} = \frac{k_A}{k_1}[A] + \frac{k_{-1}}{k_1} \quad (1)$$

$$\frac{[PS]}{[IM]} = \frac{k_B}{k_{-2}}[A] + \frac{k_2}{k_{-2}} \quad (2)$$

5. Solid-State Single-Molecule Memristor

Benefiting from this intramolecular mechanism, one individual molecule can also be used to prepare a memristor. To avoid the escape of the acyl moiety from the phenol center, a highly cross-linked polydimethoxysilane (PDMS)-containing catalyst was used to encapsulate the esterified functional center (**Figure 4**a) (detailed protocols are provided in Section S24, Supporting Information). In comparison with previous single-substrate experiments (Figure 3a,b), the long-term monitoring of Step 1 (Step 2) in the (CF_3SO_3H catalyzed) Fries rearrangement at positive (negative) biases can be realized (Figure 4b; other current signals with different catalysts are provided in Figures S45–S50, Supporting Information). Therefore, a solid-state memristor based on one individual molecule can be realized to avoid perturbation from other substrate molecules and to meet a wider range of application demands. Similar to the solution-state single-molecule memristor (Figure 2b,d), the initial stable RS (PS) state can be erased by a + 0.6 V (–0.6 V) bias pulse and written to PS (RS) by –0.05 V (+0.05 V). The +0.05 V is set as the read voltage for both the RS and PS, which leads to an instantly written RS before reading (Figure 4d). Note that the added benefit of the solid-state single-molecule memristor is the lower erased voltage (which is also supported by Figure 4f,g, and Figures S45–S50, Supporting Information), which can be attributed to the deshielding of the polar substrate and solvent molecules (aligned along the electric field).[35,38]

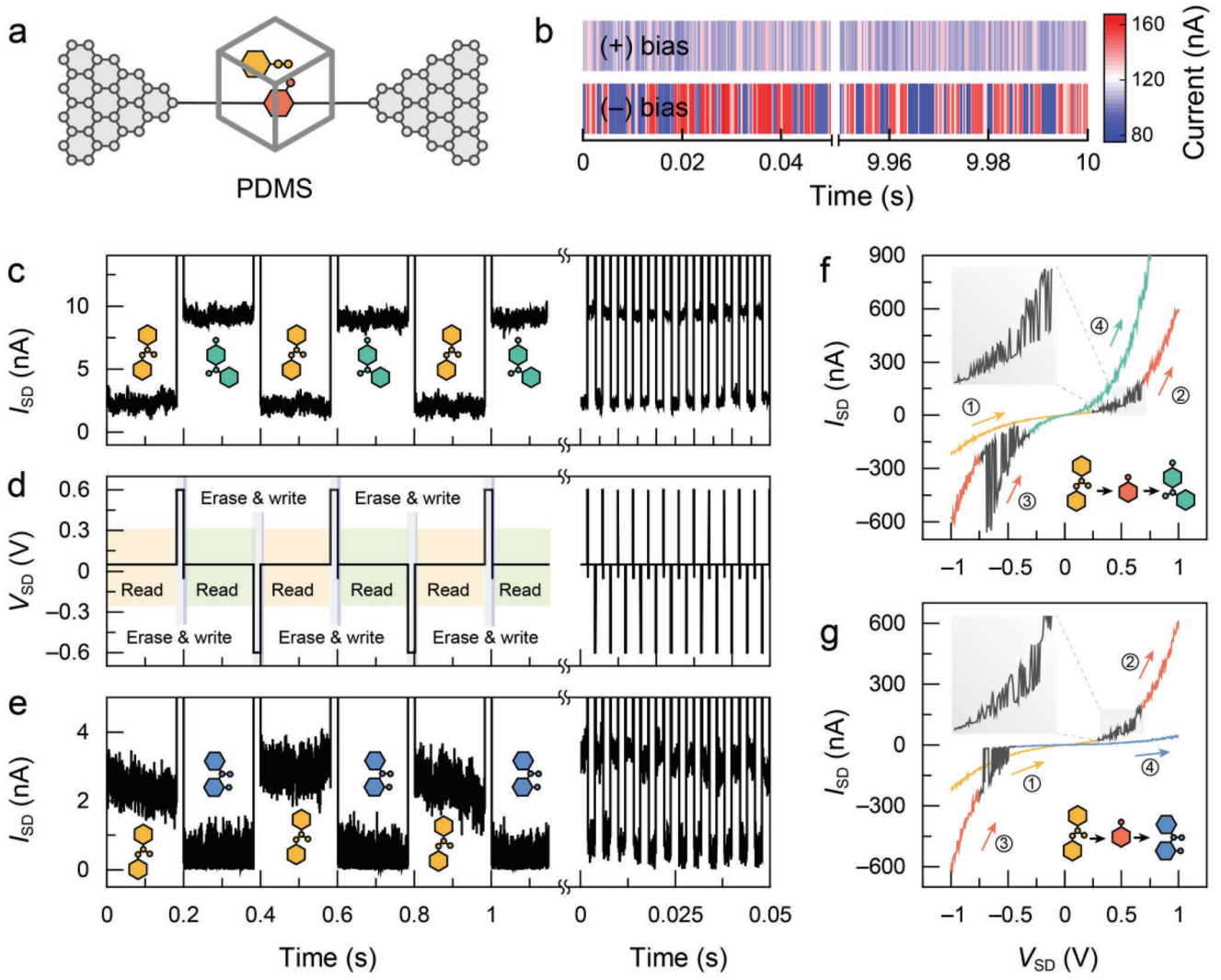

Figure 4. Solid-state single-molecule memristor. a) Schematic of the solid-state single-molecule memristor: An individual molecule was encapsulated in PDMS. b) Long-term monitoring of the encapsulated single substrate (product) under +0.3 V (–0.3 V). c) Recorded current signals during the read–erase–write–read operation to the solid-state single-molecule memristor with the catalysis by polyphosphoric acid. Right: Corresponding high-frequency read–erase–write–read operations during 0.05 s. d) Applied operation voltages and schematic of the corresponding state on the energy profile. Right: Corresponding operation voltages for the high-frequency read–erase–write–read operation. e) Recorded current signals during the read–erase–write–read operation to the solid-state single-molecule memristor with the catalysis by $TiCl_4$. Right: Corresponding high-frequency read–erase–write–read operations during 0.05 s. The IM states were observed at ≈500 nA, which are not shown in Figure 4d,e. f) Typical two-times consecutive *I*–*V* scans (①②③④) of the solid-state single-molecule with the existence of polyphosphoric acid. Inset: The enlarged binary switching in the first scan. g) Typical two-times consecutive *I*–*V* scans (①②③④) of the solid-state single-molecule with the existence of $TiCl_4$. Inset: Enlarged binary switching in the first scan.

According to the directing *ortho*- (*para*-) binding sites by $TiCl_4$ (polyphosphoric acid), multilevel switching can also be realized (Figure 4c,e), which inspires the precise target resistance approached by the well-designed molecular structure (the corresponding *G*–*t* curves of Figure 4c–e are provided in Figure S51, Supporting Information). In particular, a pair of molecules involving electron constructive and destructive quantum interference[39] can be adopted to obtain a large on/off ratio in the future. Similar to the hysteresis characteristics of conventional memristors, two consecutive *I*–*V* scans (–1 to +1 V) show the operating parameters of this single-molecule memristor (Figure 4f,g): Low (non) electric input for reading (retain), high input for erasing, switching direction for writing, and middle input (e.g., 0.1 V < |*V*| < 0.5 V) to monitor the inherent Fries rearrangement. In addition, over 2000 high-frequency write–erase operations in 10 s are achieved in this device, showing robust resistance switching based on the structural reconfiguration (Figures S52 and S53, Supporting Information). Owing to the high energy barrier of both Steps 1 and 2, the encapsulated single-molecule memristor can permanently retain the previous memory state without electric input. We are therefore confident that highly integrated arrays of single-molecule memristors can be used to construct a new generation of artificial neural network-based computing models.

6. Conclusion

A single-molecule memristor was demonstrated based on the dynamic reconfiguration of an acyl moiety on the phenol center after a comprehensive understanding of Fries rearrangement. The long-term controversial mechanistic pathway of the Fries rearrangement was clarified via a single-molecule junction. Intra-/intermolecular routes were supported by single-substrate/intermediate-molecule measurements as well as concentration-dependent measurements. The bias voltage shows high pathway selectivity for the rearrangement, which is convenient for splitting the continuous process into multiple elementary steps for independent study, a useful advantage of such a single-molecule electrical platform. More importantly, precise manipulation of the potential energy surface by the bias voltage can retain and switch the corresponding desired species along the reaction coordinate to achieve a memory effect. The memristive behaviors derived from the molecular structure reconfiguration result in long-lasting retained memory states, high write–erase endurance and operating frequency, and an adjustable on/off ratio, which inspires the development of a new generation of memristive devices and computing models.

Supporting Information

Supporting Information is available from the Wiley Online Library or from the author.

Acknowledgements

Y.G., C.Y., and S.Z. contributed equally to this work. The authors thank Zitong Liu and Deqing Zhang for providing molecular materials. The authors acknowledge primary financial support from the National Key R&D Program of China (2017YFA0204901 and 2021YFA1200101), the National Natural Science Foundation of China (22150013, 21727806, and 21933001), the Tencent Foundation through the XPLORER PRIZE, the Natural Science Foundation of Beijing (2222009), and "Frontiers Science Center for New Organic Matter" at Nankai University (Grant Number 63181206). S.Z. and Z.L. appreciate the support from the High-Performance Computing Platform of the Center for Life Science (Peking University) and High-performance Computing Platform of Peking University.

Conflict of Interest

The authors declare no conflict of interest.

Data Availability Statement

The data that support the findings of this study are available from the corresponding author upon reasonable request.

Keywords

Fries rearrangement, intra- and intermolecular pathway, single-molecule memristors, structure reconfiguration

Received: May 28, 2022
Revised: July 15, 2022
Published online:

[1] M. A. Zidan, J. P. Strachan, W. D. Lu, *Nat. Electron.* **2018**, *1*, 22.
[2] Q. Xia, J. J. Yang, *Nat. Mater.* **2019**, *18*, 309.
[3] Y. Hou, X. Hou, *Science* **2021**, *373*, 628.
[4] Q. A. Vu, H. Kim, V. L. Nguyen, U. Y. Won, S. Adhikari, K. Kim, Y. H. Lee, W. J. Yu, *Adv. Mater.* **2017**, *29*, 1703363.
[5] C. R. Peiris, S. Ferrie, S. Ciampi, W. D. A. Rickard, N. Darwish, *ACS Appl. Nano Mater.* **2022**, *5*, 6609.
[6] A. Mehonic, A. L. Shluger, D. Gao, I. Valov, E. Miranda, D. Ielmini, A. Bricalli, E. Ambrosi, C. Li, J. J. Yang, Q. Xia, A. J. Kenyon, *Adv. Mater.* **2018**, *30*, 1801187.
[7] E. Lörtscher, J. W. Ciszek, J. Tour, H. Riel, *Small* **2006**, *2*, 973.
[8] V. Meded, A. Bagrets, A. Arnold, F. Evers, *Small* **2009**, *5*, 2218.
[9] H. B. Li, B. E. Tebikachew, C. Wiberg, K. Moth-Poulsen, J. Hihath, *Angew. Chem., Int. Ed.* **2020**, *59*, 11641.
[10] D. B. Strukov, G. S. Snider, D. R. Stewart, R. S. Williams, *Nature* **2008**, *453*, 80.
[11] L. O. Chua, *Nat. Electron.* **2018**, *1*, 322.
[12] *Nat. Electron.* **2018**, *1*, 261.
[13] Y. van de Burgt, A. Melianas, S. T. Keene, G. Malliaras, A. Salleo, *Nat. Electron.* **2018**, *1*, 386.
[14] C. C. Jia, A. Migliore, N. Xin, S. Y. Huang, J. Y. Wang, Q. Yang, S. P. Wang, H. L. Chen, D. M. Wang, B. Y. Feng, Z. R. Liu, G. Y. Zhang, D. H. Qu, H. Tian, M. A. Ratner, H. Q. Xu, A. Nitzan, X. F. Guo, *Science* **2016**, *352*, 1443.
[15] L. Meng, N. Xin, C. Hu, H. A. Sabea, M. Zhang, H. Jiang, Y. Ji, C. Jia, Z. Yan, Q. Zhang, L. Gu, X. He, P. Selvanathan, L. Norel, S. Rigaut, H. Guo, S. Meng, X. Guo, *Nat. Commun.* **2022**, *13*, 1410.
[16] H. Song, Y. Kim, Y. H. Jang, H. Jeong, M. A. Reed, T. Lee, *Nature* **2009**, *462*, 1039.
[17] N. Xin, C. Hu, H. Al Sabea, M. Zhang, C. Zhou, L. Meng, C. Jia, Y. Gong, Y. Li, G. Ke, X. He, P. Selvanathan, L. Norel, M. A. Ratner, Z. Liu, S. Xiao, S. Rigaut, H. Guo, X. Guo, *J. Am. Chem. Soc.* **2021**, *143*, 20811.
[18] L. Zhang, Y.-J. Yu, L.-G. Chen, Y. Luo, B. Yang, F.-F. Kong, G. Chen, Y. Zhang, Q. Zhang, Y. Luo, J.-L. Yang, Z.-C. Dong, J. G. Hou, *Nat. Commun.* **2017**, *8*, 580.
[19] K. Zhang, C. Wang, M. Zhang, Z. Bai, F.-F. Xie, Y.-Z. Tan, Y. Guo, K.-J. Hu, L. Cao, S. Zhang, X. Tu, D. Pan, L. Kang, J. Chen, P. Wu, X. Wang, J. Wang, J. Liu, Y. Song, G. Wang, F. Song, W. Ji, S.-Y. Xie, S.-F. Shi, M. A. Reed, B. Wang, *Nat. Nanotechnol.* **2020**, *15*, 1019.
[20] C. Yang, Z. T. Liu, Y. W. Li, S. Y. Zhou, C. X. Lu, Y. L. Guo, M. Ramirez, Q. Z. Zhang, Y. Li, Z. R. Liu, K. N. Houk, D. Q. Zhang, X. F. Guo, *Sci. Adv.* **2021**, *7*, eabf0689.
[21] C. Yang, L. Zhang, C. Lu, S. Zhou, X. Li, Y. Li, Y. Yang, Y. Li, Z. Liu, J. Yang, K. N. Houk, F. Mo, X. Guo, *Nat. Nanotechnol.* **2021**, *16*, 1214.
[22] H. P. Lu, L. Xun, X. S. Xie, *Science* **1998**, *282*, 1877.
[23] K. Fries, G. Finck, *Chem. Ber.* **1908**, *41*, 4271.
[24] H. Kim, K.-I. Min, K. Inoue, J. Im Do, D.-P. Kim, J.-i. Yoshida, *Science* **2016**, *352*, 691.
[25] Y. Ogata, H. Tabuchi, *Tetrahedron* **1964**, *20*, 1661.
[26] K. v. Auwers, W. Mauss, *Justus Liebigs Ann. Chem.* **1928**, *464*, 293.
[27] N. Cohen, R. J. Lopresti, T. H. Williams, *J. Org. Chem.* **1978**, *43*, 3723.
[28] A. W. Ralston, M. R. McCorkle, E. W. Segebrecht, *J. Org. Chem.* **1941**, *6*, 750.
[29] E. H. Cox, *J. Am. Chem. Soc.* **1930**, *52*, 352.

[30] J. L. Boyer, J. E. Krum, M. C. Myers, A. N. Fazal, C. T. Wigal, *J. Org. Chem.* **2000**, *65*, 4712.
[31] A. F. Marey, F. G. Baddar, W. I. Awad, *Nature* **1953**, *172*, 1186.
[32] R. Baltzly, W. S. Ide, A. P. Phillips, *J. Am. Chem. Soc.* **1955**, *77*, 2522.
[33] A. Warshawsky, R. Kalir, A. Patchornik, *J. Am. Chem. Soc.* **1978**, *100*, 4544.
[34] X. Huang, C. Tang, J. Li, L.-C. Chen, J. Zheng, P. Zhang, J. Le, R. Li, X. Li, J. Liu, Y. Yang, J. Shi, Z. Chen, M. Bai, H.-L. Zhang, H. Xia, J. Cheng, Z.-Q. Tian, W. Hong, *Sci. Adv.* **2019**, *5*, eaaw3072.
[35] A. C. Aragonès, N. L. Haworth, N. Darwish, S. Ciampi, N. J. Bloomfield, G. G. Wallace, I. Diez-Perez, M. L. Coote, *Nature* **2016**, *531*, 88.
[36] C. Jia, X. Guo, *Chem. Soc. Rev.* **2013**, *42*, 5642.
[37] S. M. Hubig, J. K. Kochi, *J. Am. Chem. Soc.* **2000**, *122*, 8279.
[38] L. Xu, E. I. Izgorodina, M. L. Coote, *J. Am. Chem. Soc.* **2020**, *142*, 12826.
[39] J. Bai, A. Daaoub, S. Sangtarash, X. Li, Y. Tang, Q. Zou, H. Sadeghi, S. Liu, X. Huang, Z. Tan, J. Liu, Y. Yang, J. Shi, G. Mészáros, W. Chen, C. Lambert, W. Hong, *Nat. Mater.* **2019**, *18*, 364.